Chemical Engineering Journal 263 (2015) 55–61

Contents lists available at ScienceDirect

Chemical Engineering Journal

journal homepage: www.elsevier.com/locate/cej

# Manipulating the morphology of nanoscale zero-valent iron on pumice for removal of heavy metals from wastewater

Tingyi Liu [a], Zhong-Liang Wang [a,b,*], Yanqiu Sun [a]

[a] Tianjin Key Laboratory of Water Resources and Environment, Tianjin Normal University, Tianjin 300387, China
[b] State Key Laboratory of Environmental Geochemistry, Institute of Geochemistry, Chinese Academy of Sciences, Guiyang 550002, China

## HIGHLIGHTS

- Manipulating the morphology of nanoscale zero-valent iron on pumice.
- The effective removal of heavy metals from wastewater using P-NZVI.
- The kinetics and thermodynamics of heavy metals by the efficient composite.
- An effective technology for in situ remediation to heavy metals.

## ARTICLE INFO

*Article history:*
Received 16 September 2014
Received in revised form 6 November 2014
Accepted 7 November 2014
Available online 15 November 2014

*Keywords:*
Nanoscale zero-valent iron
Pumice
Mercury (II)
Chromium (VI)

## ABSTRACT

The removal of heavy metals from wastewater is one of the most important issues for the world, especially from industrial effluents. Pumice-nanoscale zero-valent iron (P-NZVI) was successfully prepared in different experimental conditions. Meanwhile, the shape, size and distribution of NZVI on P-NZVI were evaluated using a scanning electron microscope (SEM). At the optimum condition, NZVI with a mean diameter of 20.2 nm was distributed uniformly and consistently on the surface of pumice. Freundlich isotherm analysis suggested that the surface property of P-NZVI were heterogeneous. The removal of Hg (II) and Cr (VI) by P-NZVI could be well described by pseudo-first-order kinetic model. At equilibrium $q_{max}$ of Hg (II) and Cr (VI) was 107.1 and 106.9 mg/g, respectively. Thermodynamic investigation suggested that the removal of Hg (II) and Cr (VI) by P-NZVI was an endothermic and spontaneous process. The less values of $\Delta H^0$ for Hg (II) than those for Cr (VI) demonstrated that more thermal energy was needed to remove Cr (VI) than Hg (II) at the same reaction rate.



## 1. Introduction

The presence of heavy metals in wastewater will contaminate the water environment. Furthermore, the wastewater which has not been handled properly will pose an admitted hazard to human health and the environment. Hence, heavy metals must be removed from wastewater to bring their concentrations down to below the prescribed legal limit.

Pumice is a porous material with large surface area, which can provide more reaction sites for heavy metals thus leading to the removal of heavy metals from wastewater [1]. Pumice can be used as an efficient low-cost adsorbent for heavy metals [2]. Furthermore, pumice particles were effective as a support media in filtration and heterogeneous catalytic reactions [3,4]. Iron-coated pumice performed well both in maintaining the long-term hydraulic conductivity and eliminating contaminants [5].

As is well known, nanoscale zero-valent iron (NZVI) was effective to remove pollutants from wastewater because of its extremely small particle size, large surface area and high reactivity [6,7]. However, the application of NZVI is primarily restricted to anaerobic condition since it is easily oxidized to iron oxides under aerobic condition [8]. Also, the easy formation of their agglomerates restricted field applications of NZVI [9]. To overcome these problems, NZVI has been modified using surface stabilizers such as chitosan [10], guar gum [11], and starch [12]. In order to enhance the stability in the air, NZVI was supported on PolyFlo resin [13]. In recent years, porous materials, including pillared clay [14], bentonite [15], chitosan beads [16] and kaolinite [17], have been widely used to enhance the dispersibility of NZVI particles. Pumice can be also used as a porous material to support and stabilize iron [18,19]. Pumice is a commonly available rock with a stable

* Corresponding author at: Tianjin Key Laboratory of Water Resources and Environment, Tianjin Normal University, Tianjin 300387, China. Tel./fax: +86 22 23766256.
*E-mail address:* wangzhongliang@vip.skleg.cn (Z.-L. Wang).

http://dx.doi.org/10.1016/j.cej.2014.11.046
1385-8947/

structure and low cost [2], which could potentially be used as a porous material to support NZVI to remove heavy metals from contaminated water. Several supporting materials were used to support NZVI particles and enhance their dispersibility, however, only a few studies have focused on the influence of the different experimental conditions on the morphology of NZVI.

The objective of the study is to demonstrate that NZVI can be effectively supported on pumice (P-NZVI) with significant enhancement of its decontamination ability. Effectiveness of P-NZVI in contaminant remediation was examined with Hg (II) and Cr (VI) as the test contaminant. P-NZVI composite was successfully prepared in different experimental conditions and the influence of these conditions on the morphology of NZVI on P-NZVI was evaluated with scanning electron microscope (SEM) analysis. The impact of different factors on the kinetics of heavy metals reduction from wastewater by P-NZVI, as well as the thermodynamics study, was investigated.

## 2. Materials and methods

### 2.1. Materials

Sodium borohydride ($NaBH_4$) and iron chloride hexahydrate ($FeCl_3{\cdot}6H_2O$) were provided by Fuchen Chemical Reagent Manufactory (Tianjin, China). Pumice with a mean diameter of 1.0 mm was purchased from Kexin Building Materials Co., Ltd. (Shijiazhuang, China). $K_2CrO_4$ and $HgCl_2$ were provided by Jinbohua Laboratory Equipment Co., Ltd. (Tianjin, China). All other chemicals were of analytical grade purity.

### 2.2. Preparation of P-NZVI

The effect of the mass ratio of Fe (III) to pumice, the molar ratio of Fe (III) to $BH_4^-$, and the volume ratio of deionized water to absolute alcohol on the morphology of NZVI on P-NZVI was investigated. P-NZVI was prepared according to the procedures described in detail elsewhere [17,19]. Briefly, a known mass of pumice was initially placed into a three-necked flask, and a ferric solution was added and stirred for 1 h. Subsequently, a freshly prepared $NaBH_4$ solution was added at a rate of 50–60 drops per minute into the mixture. Every 10 min, the mixture was sonicated for 2 min. After the completed addition of $NaBH_4$ solution, a constant stirring continued for 60 min. The prepared composite was separated from the liquid solution, and then it was dried at 65 °C for 24 h [10]. The prepared material was stored in brown and sealed bottles for further use. The whole process was carried out in a nitrogen atmosphere.

### 2.3. Batch experiments

Batch experiments for removal of heavy metals by P-NZVI were carried out in polytetrafluoroethylene bottles at room temperature without mechanical agitation. To each bottle, 100 mL wastewater and P-NZVI were added. At certain time-interval, 1 mL sample was withdrawn using disposable syringes and filtered through a 0.42 μm micro-hole filter. All experiments were performed in duplicate.

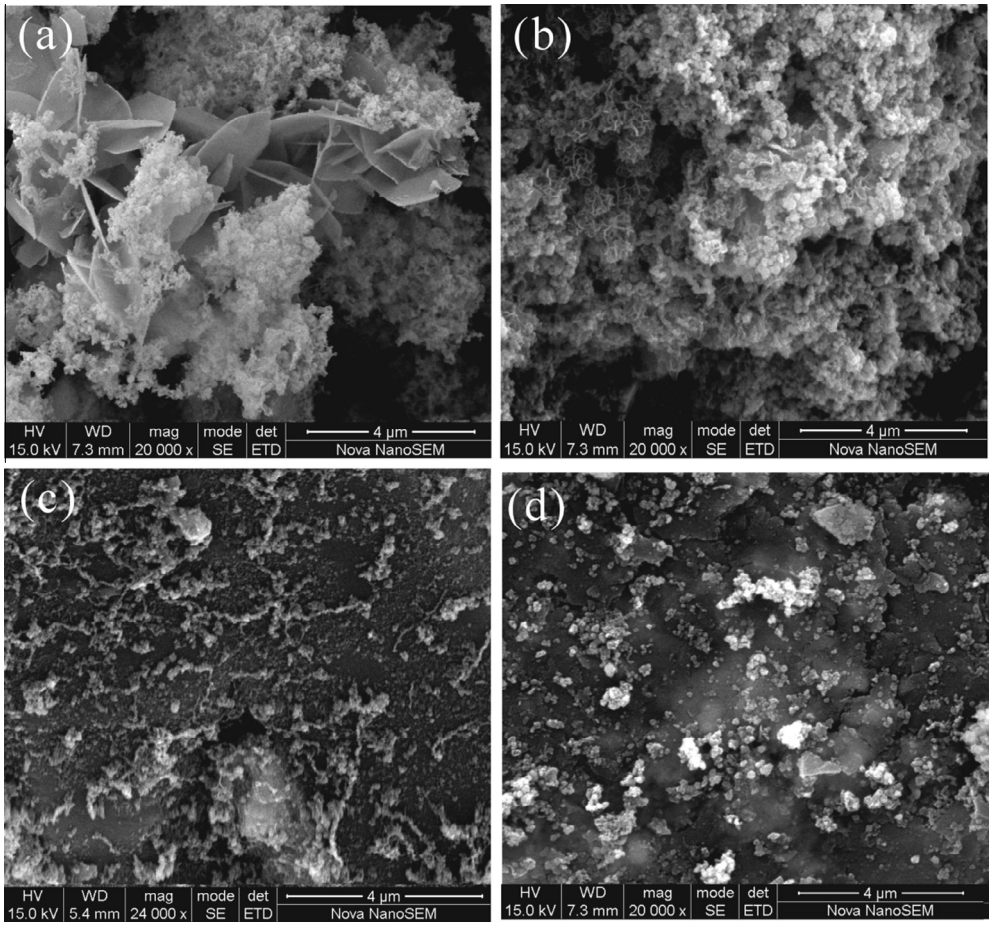


**Fig. 1.** Effect of the masse ratio of Fe (III) to pumice on the morphology of NZVI on P-NZVI: (a) 1:3, (b) 1:6, (c) 1:9 and (d) 1:12.

### 2.4. Kinetics and thermodynamic o f Hg (II) and Cr (VI) removal by P-NZVI

The effect of pH value (3.11, 4.12, 5.17, 6.10, 7.05 and 8.13) and NZVI dosages (0.28, 0.373, 0.56, and 1.12 g) on the reduction kinetics of Hg (II) and Cr (VI) was studied in accordance with a previously reported procedure [20,21].

The thermodynamic parameters such as enthalpy change ($\Delta H^0$), Gibbs free energy change ($\Delta G^0$) and entropy change ($\Delta S^0$) were employed to evaluate the feasibility and nature of the adsorption process.

The enthalpy change ($\Delta H^0$) for the adsorption heavy metals by P-NZVI was calculated using the following equation [20]:

$$\ln C_e = \Delta H^0/(RT) + K_0 \quad (1)$$

where $T$ is the solution temperature (K), $R$ is gas constant (8.314 kJ/(mol K)) and $K_0$ is a constant. The values of $\Delta H^0$ were calculated by plotting $\ln C_e$ versus $1/T$.

The Gibbs free energy change ($\Delta G^0$) for the adsorption heavy metals by P-NZVI was calculated using the following equation [22]:

$$\Delta G^0 = -nRT \quad (2)$$

where $n$ is a Freundlich isotherm constant.

The entropy change ($\Delta S^0$) was computed using the relationship [20]:

$$\Delta S^0 = (\Delta H^0 - \Delta G^0)/T \quad (3)$$

### 2.5. Characterization and analytical methods

The P-NZVI was placed at a platform with a diameter of 5 cm and gold-coated by a vacuum electric sputter coater to a thickness of 600 Å. Then, the morphological analysis of P-NZVI was performed using a scanning electron microscope (SEM) (SEM, FEI Nova NanoSEM 230) with a high resolution of 3.0 nm under high vacuum at 15 keV. The concentrations of Hg (II) and Cr (VI) in the solution were measured using inductively coupled plasma-mass spectrometry (ICP-MS, Elan-9000, PE). The procedure was as follows: firstly, 1 mL sample was pipetted into a 10 mL comparator with cover using disposable syringes. Secondly, the sample was diluted to volume using 3% $HNO_3$ as the acid medium. Then, the concentrations of Hg (II) and Cr (VI) in the solution were measured using ICP-MS.

## 3. Results and discussion

### 3.1. SEM characterization

SEM (Figs. 1–3) images are used to qualitatively understand the morphology of NZVI on P-NZVI. The effect of the mass ratio of Fe (III)/pumice on the morphology of NZVI on P-NZVI was shown in Fig. 1. It can be seen that the mass ratio of Fe (III)/pumice has a significant effect on the diameter, shape and distribution of NZVI on P-NZVI (Fig. 1). When the ratio was 1:3, the fluffy masses and

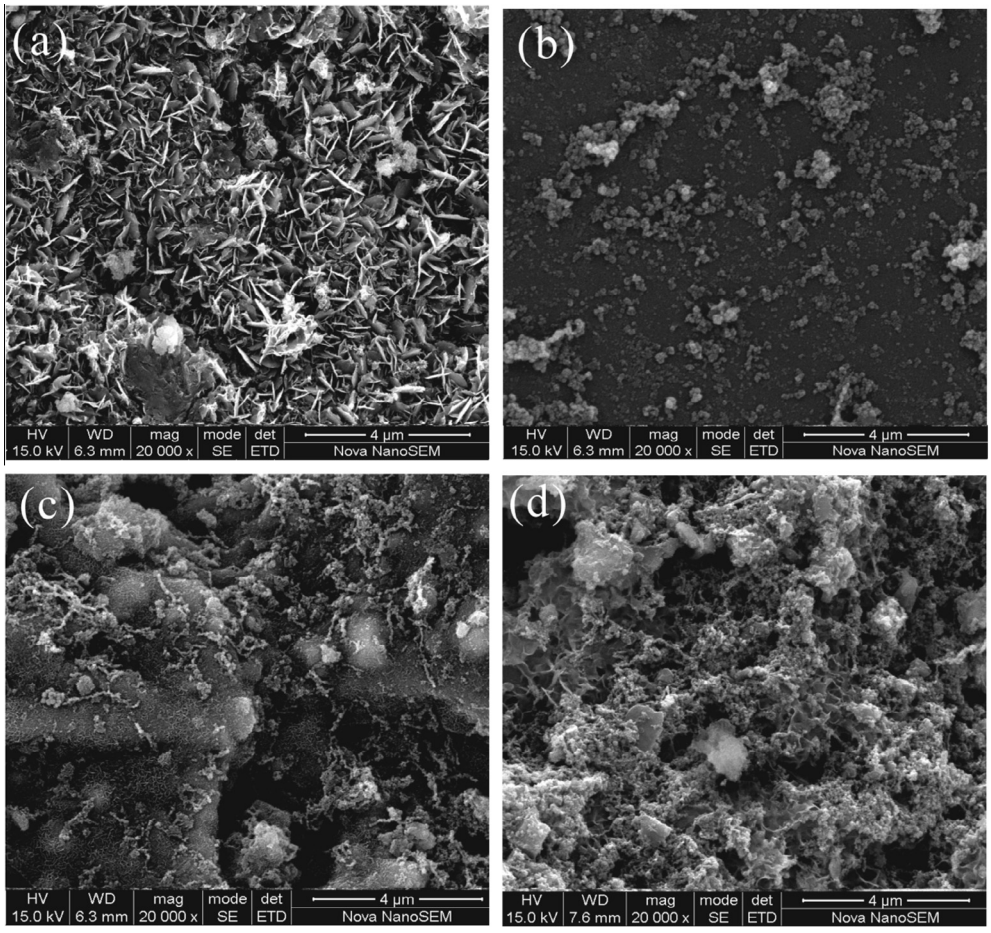


**Fig. 2.** Effect of the molar ratio of Fe (III) to $BH_4^-$ on the morphology of NZVI on P-NZVI: (a) 1:2, (b) 1:5, (c) 1:8 and (d) 1:10.

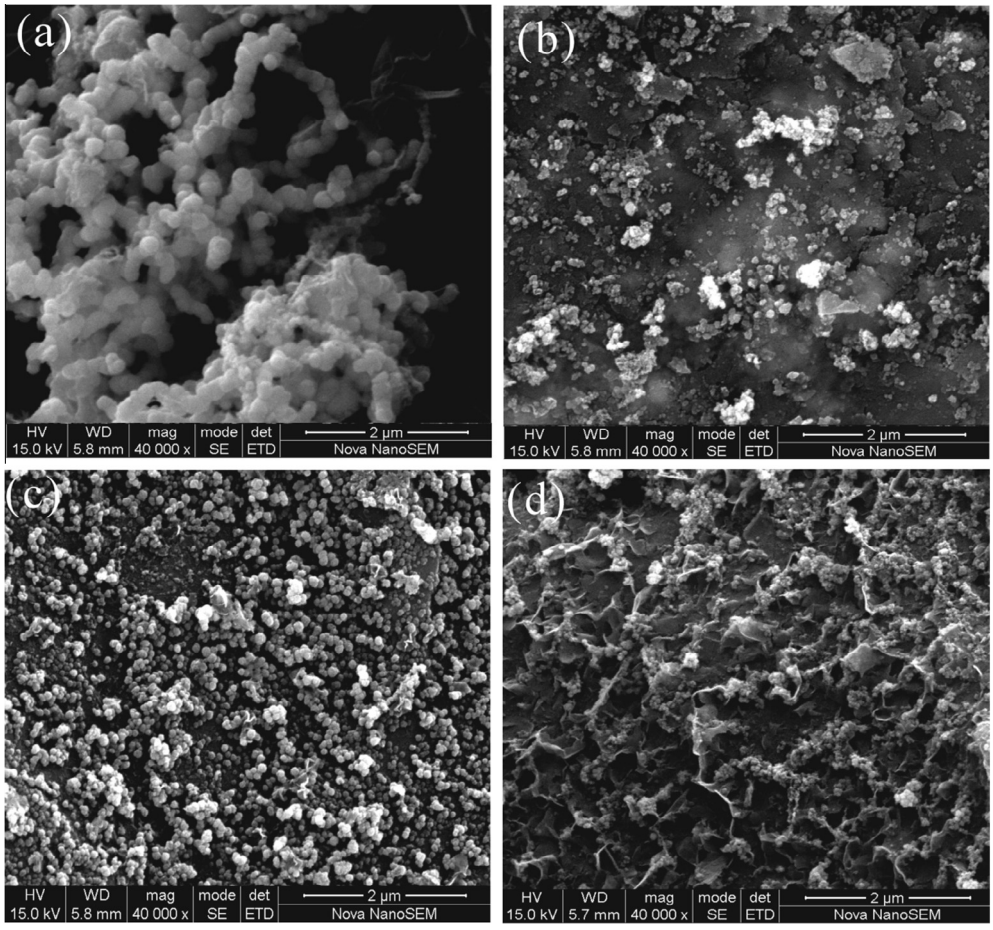


**Fig. 3.** Effect of the volume ratio of deionised (DI) water to absolute alcohol on the morphology of NZVI on P-NZVI: (a) 2:1, (b) 4:1, (c) 8:1 and (d) 12:1.

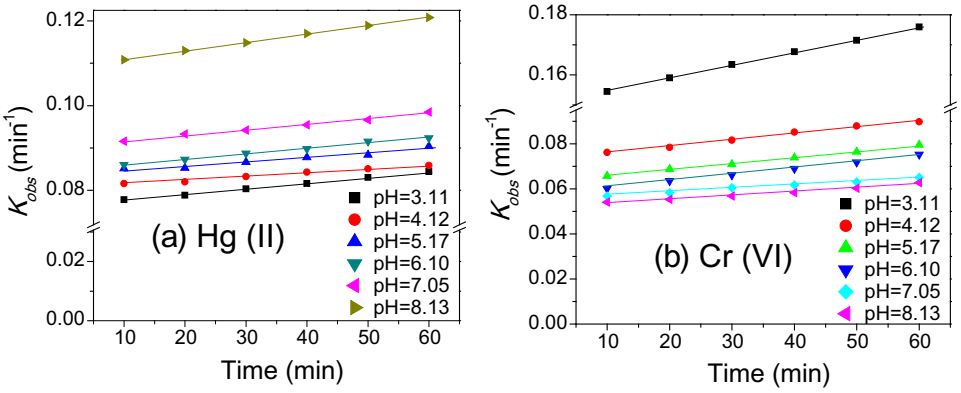


**Fig. 4.** Effect of pH values on $K_{obs}$ for (a) Hg (II) and (b) Cr (VI) reduction by P-NZVI. Initial Hg (II) and Cr (VI) concentration: 60 mg/L; the mass fraction of NZVI in P-NZVI: 7.7%, 0.28 g; pH: 3.11, 4.12, 5.17, 6.10, 7.05 and 8.13; temperature: 20 °C.

irregular plate-shaped of NZVI were formed (Fig. 1(a)). As the ratio decreased to 1:6, NZVI was mainly spherical nano-particles with a mean diameter of 12.8 nm (Fig. 1(b)). However, these NZVI particles were obviously aggregated in Fig. 1(b), leading to a decrease in its chemical activity and removal capacity of pollutants [23]. NZVI particles were not packed tightly together in Fig. 1(c), nevertheless a chainlike and aggregated structure was formed because of the natural magnetism of NZVI [24]. NZVI with a diameter of 36.9 nm was distributed uniformly on the surface of pumice when the ratio was decreased to 1:12 (Fig. 1(d)), which demonstrated that pumice can be effective to enhance the dispersibility of NZVI particles [19].

Fig. 2 showed that with the decrease in the molar ratio of Fe (III)/$BH_4^-$ from 1:2 to 1:10, there were significant changes in the diameter, shape and distribution of NZVI on P-NZVI. Strips and patches or plate-shaped iron were noticed in Fig. 2(a). Furthermore, the iron was not nano-scale particle. As the molar ratio was 1:5, NZVI with a mean diameter of 36.2 nm was distributed uniformly on the surface of pumice (Fig. 2(b)). Sodium borohydride is frequently used as the reductant in the synthesis because of the

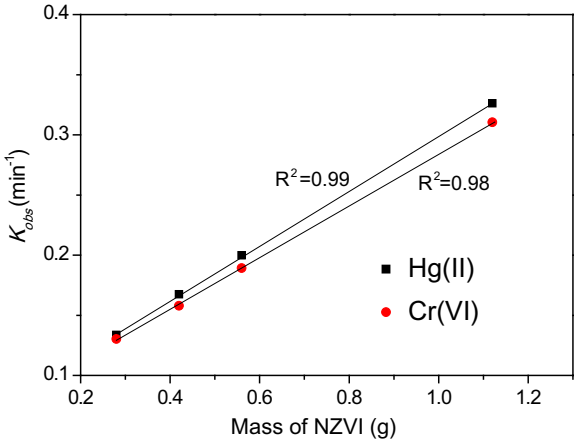


**Fig. 5.** Effect of the mass of NZVI on $K_{obs}$ for (a) Hg (II) and (b) Cr (VI) reduction by P-NZVI. Initial Hg (II) and Cr (VI) concentration: 60 mg/L; the mass of NZVI on P-NZVI: 0.28, 0.42, 0.56 and 1.12 g; pH: 6.10; temperature: 20 °C.

sufficiently low reduction potential of borohydride ion [25]. As a result, the reaction proceeded quite rapidly as an increase in the molecular fraction of $BH_4^-$. The NZVI particles became smaller in Fig. 2(c) and (d) than those in Fig. 2(b). However, the presence of high concentrations of $Na^+$ promoted agglomeration of nanoparticles [26]. Due to an increase in molecular fraction of $NaBH_4$, NZVI particles were obviously aggregated in Fig. 2(c) and (d).

The effect of the volume ratio of deionized water to absolute alcohol on the morphology of NZVI was shown in Fig. 3. At a volume ratio of 2:1, 96.8% of NZVI particles aggregated to greater than 1.5 μm and a chainlike structure was also observed (Fig. 3(a)). Conversely, when the volume ratio of deionized water to absolute alcohol was increased to 4:1, the primary (94.4%) NZVI became much smaller (18.2 nm) and was distributed uniformly on the surface of pumice in Fig. 3(b). In this case, no aggregates greater than 200 nm were detected. When the volume ratio was further increased to 8:1, NZVI was distributed uniformly and consistently on the surface of pumice in Fig. 3(c). NZVI particles were obviously uniform and regular spheres with a mean diameter of 20.2 nm, although larger aggregates with diameters around 65 nm (2%) and 116 nm (1%) were also discovered (Fig. 3(c)). When the volume ratio was finally increased to 12:1, NZVI particles became even smaller (12.7 nm) and there were still small aggregates (60 nm) detected in Fig. 3(d), however, these NZVI particles were not distributed uniformly. Smaller NZVI was obtained as an increase of the carboxymethyl cellulose (CMC)/$Fe^{2+}$ molar ratio [26]. The polymeric structure of CMC enhanced the growth of the nucleation of Fe atoms, which resulted in the formation of a larger number of smaller particles through the electrosteric stabilization [26]. The same phenomenon appeared to be plausible for the stabilization of Au nanoparticles by thiol-terminated polyethylene glycol (PEG) [27]. So far a conclusion can be drawn that the volume ratio of deionized water to absolute alcohol played an important role in the diameter and distribution of NZVI on P-NZVI.

**Table 1**
Freundlich isotherm constants for Hg (II) and Cr (VI) at different temperatures.

| $T$ (K) | Hg (II) | | | | Cr (VI) | | | |
|---|---|---|---|---|---|---|---|---|
| | $q_{max}$ | $n$ | $K$ | $R^2$ | $q_{max}$ | $n$ | $K$ | $R^2$ |
| 293 | 106.70 | 2.73 | 104.30 | 0.98 | 106.50 | 2.49 | 80.81 | 0.97 |
| 298 | 106.92 | 3.62 | 132.84 | 0.97 | 106.63 | 3.03 | 95.68 | 0.98 |
| 303 | 107.02 | 4.17 | 155.72 | 0.97 | 106.84 | 4.37 | 120.30 | 0.98 |
| 308 | 107.11 | 4.81 | 174.22 | 0.96 | 106.91 | 5.16 | 130.71 | 0.97 |

The chemical composition of pumice was 66.8% $SiO_2$, 23.1% $Al_2O_3$, 2.88% $Fe_2O_3$, 2.18% CaO and small amounts of Mn, Mg, P and S [19]. The theoretical mass fraction of NZVI in prepared P-NZVI was about 7.6%. NZVI has very thin layers of oxide shells with distinguishable gray or dark portions inside due to the $Fe^0$ [28]. The main compound on the NZVI surface was iron ferrihydroxide [29].

### 3.2. Kinetics of Hg (II) and Cr (VI) removal by P-NZVI

#### 3.2.1. Effect of pH values

The dependence of $K_{obs}$ on pH was investigated and the result was shown in Fig. 4. It can be seen that $K_{obs}$ of Hg (II) increases with an increase in the initial pH, indicating that the reduction rate increased as an increasing pH value (Fig. 4(a)). However, $K_{obs}$ of Cr (VI) decreases with an increase in the initial pH, indicating that the reduction rate decreased as pH increased (Fig. 4(b)). With an increasing pH, the surface of P-NZVI became dominantly negatively charged, leading to the enhanced attraction force between P-NZVI and Hg (II) and the repulsion force between P-NZVI and $HCrO_4^-/CrO_4^{2-}$ [19]. As a result, $K_{obs}$ of Hg (II) increases but $K_{obs}$ of Cr (VI) decreases with an increase in the initial pH. The finding is in agreement with previous works reported by other researchers [2,5,30].

#### 3.2.2. Effect of NZVI dosage

The effect of the mass of NZVI on $K_{obs}$ for Hg (II) and Cr (VI) was investigated, and the results are shown in Fig. 5. Obviously, $K_{obs}$ of Hg (II) and Cr (VI) displays a good linearity to the dosage of P-NZVI with correlation coefficients ($R^2$) more than 0.98. This indicated

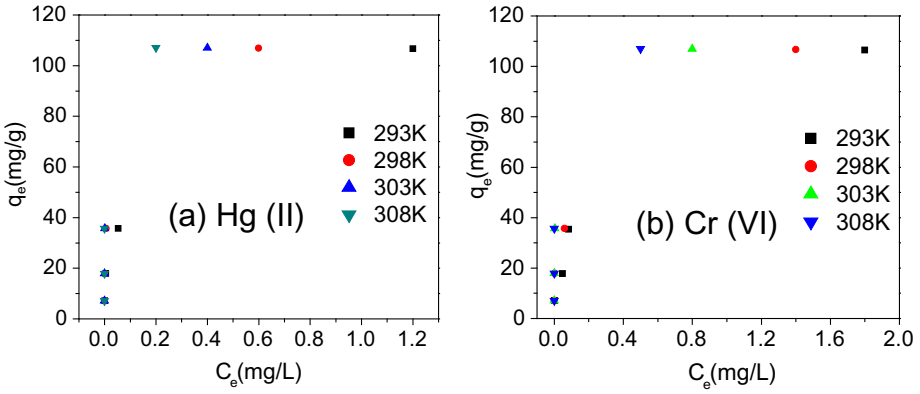


**Fig. 6.** Adsorption isotherms of (a) Hg (II) and (b) Cr (VI) onto P-NZVI.

**Table 2**
Thermodynamic parameters for adsorption of Hg (II) onto P-NZVI.

| $\Delta H^0$ (kJ/mol) | $\Delta G^0$ (kJ/mol) | | | | $\Delta S^0$ (kJ/mol) | | | |
|---|---|---|---|---|---|---|---|---|
| | 293 K | 298 K | 303 K | 308 K | 293 K | 298 K | 303 K | 308 K |
| 345.40 | −6.65 | −8.97 | −10.49 | −12.30 | 1.20 | 1.19 | 1.17 | 1.16 |
| 323.31 | −6.65 | −8.97 | −10.49 | −12.30 | 1.13 | 1.12 | 1.10 | 1.09 |
| 288.72 | −6.65 | −8.97 | −10.49 | −12.30 | 1.01 | 1.00 | 0.99 | 0.98 |
| 86.73 | −6.65 | −8.97 | −10.49 | −12.30 | 0.32 | 0.32 | 0.32 | 0.32 |

**Table 3**
Thermodynamic parameters for adsorption of Cr (VI) onto P-NZVI.

| $\Delta H^0$ (kJ/mol) | $\Delta G^0$ (kJ/mol) | | | | $\Delta S^0$ (kJ/mol) | | | |
|---|---|---|---|---|---|---|---|---|
| | 293 K | 298 K | 303 K | 308 K | 293 K | 298 K | 303 K | 308 K |
| 410.33 | −6.06 | −7.50 | −11.00 | −13.19 | 1.42 | 1.40 | 1.39 | 1.37 |
| 426.91 | −6.06 | −7.50 | −11.00 | −13.19 | 1.48 | 1.46 | 1.45 | 1.43 |
| 238.92 | −6.06 | −7.50 | −11.00 | −13.19 | 0.84 | 0.83 | 0.82 | 0.82 |
| 95.94 | −6.06 | −7.50 | −11.00 | −13.19 | 0.25 | 0.25 | 0.25 | 0.26 |

that the removal of Hg (II) and Cr (VI) by P-NZVI agreed well with the pseudo-first-order reaction kinetics under various conditions (Fig. 5). As a result of increasing dosage of NZVI, the surface area and reactive sites of NZVI were enhanced, leading to an increase of the efficiency of remediation [31]. At the same time, due to pumice with a large surface area providing more reaction sites for heavy metals [18], heavy metals can be easily introduced to NZVI on P-NZVI. This cooperative effect enhanced the removal efficiency of heavy metals. Thus, it can also be found that $K_{obs}$ are all more than 0.13 $min^{-1}$ and even high as 0.32 $min^{-1}$. The finding is consistent with the result in Fig. 3(d). It also can be seen that $K_{obs}$ of Hg (II) is more than that of Cr (VI) (Fig. 5), which may indicate that it is more quickly to remove Hg (II) than Cr (VI). The adsorption equilibrium time for Hg (II) was less than that for Cr (VI) [32].

### 3.3. Adsorption of isotherm analysis

Adsorption isotherms of Hg (II) and Cr (VI) onto P-NZVI were performed at four different temperatures (293–308 K). The initial Hg (II) and Cr (VI) concentrations were 20, 60, 100 and 300 mg/L, respectively. The results were shown in Fig. 6. It can be seen that $q_e$ of Hg (II) increases with the increase of the temperatures and $C_e$ (Fig. 6(a)). Adsorption isotherm of Cr (VI) onto P-NZVI is similar with that of Hg (II) (Fig. 6(b)). The phenomenon is in conformity with the kinetics behavior previously. The same result was reported using chitosan-NZVI beads to remove Cr (VI) [20].

### 3.4. Thermodynamic parameters

The equilibrium adsorption data on Hg (II) and Cr (VI) onto P-NZVI at different temperatures were analyzed using Freundlich model (Table 1) and the parameters of Freundlich equation were calculated from those isotherms (Tables 2 and 3).

At different temperatures, the values of $q_{max}$ of Hg (II) can be estimated to be 106.7, 106.9, 107.0 and 107.1 mg/g, respectively (Table 1). Likewise, the values of $q_{max}$ of Cr (VI) are 106.5, 106.6, 106.8 and 106.9 mg/g, respectively (Table 1), which are much higher than those reported in other NZVI system [20]. According to the fact that the parameter $n > 1$ represents a favorability adsorption condition [33], all of the exponent $n$ are larger than 2.4 for adsorption of Hg (II) and Cr (VI) on P-NZVI (Table 1), which indicated that the removal of Hg (II) and Cr (VI) by P-NZVI could easily happened. As shown in Table 1, the values of Freundlich isotherm constant $K$ are all more than 80 at four temperatures. At the same time, the values of $K$ increased as an increase in temperatures indicating that the affinity of Hg (II) and Cr (VI) to P-NZVI increased as the temperatures increased. This phenomenon may also help us explain the kinetics behavior previously. Hence, the results show that Freundlich isotherm provides a good model of the sorption system, which is based on heterogeneous adsorption of metal ions. The high correlation coefficients ($R^2 > 0.962$) also suggested that Freundlich isotherm agreed well with experimental data. The analysis hence suggested that P-NZVI were heterogeneous in the surface properties. This is in agreement with the results shown in Figs. 1–3.

At the reaction temperature of 293–308 K, the $\Delta G^0$ for Hg (II) adsorption process was found to be −6.65, −8.97, −10.49 and −12.30 kJ/mol, respectively (Table 2). The negative values of $\Delta G^0$ (Table 2) suggested that the process was spontaneous. The values of $\Delta G^0$ decreased with an increase in temperature, indicating that the Hg (II) adsorption was more favorable at higher temperature, a phenomenon also observed by Wu and Li [34]. The positive values of $\Delta H^0$ suggested that Hg (II) removal by P-NZVI was an endothermic process, which was in agreement with previous observation, namely $K_{obs}$ increased with an increase in temperature. The positive values of $\Delta S^0$ for all case (Table 2) reflected the good affinity of the sorbent for Hg (II) ions and the increasing randomness at the solid-solution interface during the adsorption of Hg (II). The positive values of $\Delta S^0$ suggested some structural changes in Hg (II) (adsorbate) and P-NZVI (adsorbent) [35]. The same phenomena had also been reported for the system of Cr (VI) on chitosan-NZVI beads, as well as basic dyes on tree fern [20,36].

The similar regularity was also found on Cr (VI) adsorption process (Table 3). The thermodynamic parameters showed that reactions were endothermic and spontaneous in nature. $\Delta H^0$ for Hg (II) was less than that for Cr (VI) at the same condition (Tables 2 and 3), which demonstrated that more thermal energy was needed to remove Cr (VI) than Hg (II) at the same reaction rate. This is consistent with the result of Fig. 5. Adsorption of $\beta$-carotene onto carbon coated monolith was spontaneous and endothermic [37].

## 4. Conclusions

In this study, P-NZVI was successfully prepared and used to remove heavy metals from wastewater. Kinetics and thermodynamics of Hg (II) and Cr (VI) removal from wastewater by P-NZVI were investigated. Based on the results, the major findings are summarized as follows:

- SEM results showed that the mass ratio of Fe (III) to pumice, the molar ratio of Fe (III) to $BH_4^-$, and the volume ratio of deionized water to absolute alcohol played an important role in the shape, diameter and distribution of NZVI on P-NZVI.
- $K_{obs}$ for Hg (II) increased with increasing NZVI dosage and pH values, however, $K_{obs}$ for Cr (VI) increased with increasing NZVI dosage but decreased with the increase in pH values.
- $q_e$ of Hg (II) and Cr (VI) increases with the increase of the temperatures and $C_e$.
- Freundlich isotherm analysis suggested that P-NZVI were heterogeneous in the surface properties.
- Thermodynamic investigation showed that enthalpy change ($\Delta H^0$) was positive, indicating that the removal of Hg (II) than Cr (VI) was an endothermic process. The negative values of Gibbs free energy change ($\Delta G^0$) for Hg (II) and Cr (VI) suggested that the process was spontaneous.

The result revealed that P-NZVI had the capacity to remediate wastewater containing heavy metals. Our study was to provide information for engineers on using NZVI in the practical remediation of wastewater. P-NZVI could become an effective and promising technology for in situ remediation of wastewater.

## Acknowledgments

The authors thank Zhigang Zhang, Qian Wang and Yuntao Shang for their support with analyses. This work was financially supported by National Science & Technology Pillar Program (2012BAC07B02), the Innovation Team Training Plan of the Tianjin Education Committee (TD12-5037), National Natural Science Foundation of China (21307090) and Tianjin Municipal Natural Science Foundation of China (14JCZDJC41000).

## References

[1] T. Candy, C.P. Sharma, Chitosan matrix for oral sustained delivery of ampicillin, Biomaterials 14 (1993) 939–944.
[2] M. Yavuz, F. Gode, E. Pehlivan, S. Ozmert, Y.C. Sharma, An economic removal of $Cu^{2+}$ and $Cr^{3+}$ on the new adsorbents: pumice and polyacrylonitrile/pumice composite, Chem. Eng. J. 137 (2008) 453–461.
[3] B. Farizoglu, A. Nuhoglu, E. Yildiz, B. Keskinler, The performance of pumice as a filter bed material under rapid filtration conditions, Filtr. Sep. 40 (2003) 41–46.
[4] A. Rachel, B. Lavedrine, M. Subrahmanyam, P. Boule, Use of porous lavas as supports of photocatalysts, Catal. Commun. 3 (2002) 165–171.
[5] N. Moraci, P.S. Calabrò, Heavy metals removal and hydraulic performance in zero-valent iron/pumice permeable reactive barriers, J. Environ. Manage. 91 (2010) 2336–2341.
[6] W. Zhang, Nanoscale iron particles for environmental remediation: an overview, J. Nanopart. Res. 5 (2003) 323–332.
[7] S.R. Kanel, J.M. Greneche, H. Choi, Arsenic (V) removal from groundwater using nanoscale zero-valent iron as a colloidal reactive barrier material, Environ. Sci. Technol. 40 (6) (2006) 2045–2050.
[8] J.T. Nurmi, P.G. Tratnyek, V. Sarathy, D.R. Baer, J.E. Amonette, K. Pecher, C. Wang, J.C. Linehan, D.W. Matson, R.L. Penn, M.D. Driessen, Characterization and properties of metallic iron nanoparticles: spectroscopy, electrochemistry, and kinetics, Environ. Sci. Technol. 39 (5) (2005) 1221–1230.
[9] X. Zhang, S. Lin, Z. Chen, M. Megharaj, R. Naidu, Kaolinite-supported nanoscale zero-valent iron for removal of $Pb^{2+}$ from aqeous solution: reactivity, characterization and mechanism, Water Res. 45 (2011) 3481–3488.
[10] B. Geng, Z.H. Jin, T.L. Li, X.H. Qi, Kinetics of hexavalent chromium removal from water by chitosan-$Fe^0$ nanoparticles, Chemosphere 75 (2009) 825–830.
[11] A. Tiraferri, K.L. Chen, R. Sethi, M. Elimelech, Reduced aggregation and sedimentation of zero-valent iron nanoparticles in the presence of guar gum, J. Colloid Interface Sci. 324 (2008) 71–79.
[12] F. He, D. Zhao, Preparation and characterization of a new class of starch-stabilized bimetallic nanoparticles for degradation of chlorinated hydrocarbons in water, Environ. Sci. Technol. 39 (2005) 3314–3320.
[13] S.M. Ponder, J.C. Darab, T.E. Mallouk, Remediation of Cr (VI) and Pb (II) aqueous solutions using supported, nanoscale zero-valent iron, Environ. Sci. Technol. 34 (2000) 2564–2569.
[14] Y. Zhang, Y. Li, J. Li, L. Hu, X. Zheng, Enhanced removal of nitrate by a novel composite: nanoscale zero valent iron supported on pillared clay, Chem. Eng. J. 171 (2011) 526–531.
[15] L.N. Shi, X. Zhang, Z.L. Chen, Removal of chromium (VI) from wastewater using bentonite-supported nanoscale zero-valent iron, Water Res. 45 (2) (2011) 886–892.
[16] T. Liu, X. Yang, Z.L. Wang, X. Yan, Enhanced chitosan beads-supported $Fe^0$-nanoparticles for removal of heavy metals from electroplating wastewater in permeable reactive barriers, Water Res. 47 (17) (2013) 6691–6700.
[17] C. Uzum, T. Shahwan, A.E. Erolu, K.R. Hallam, T.B. Scott, I. Lieberwirth, Synthesis and characterization of kaolinite-supported zero-valent iron nanoparticles and their application for the removal of aqueous $Cu^{2+}$ and $Co^{2+}$ ions, Appl. Clay Sci. 43 (2) (2009) 172–181.
[18] M. Kitis, S.S. Kaplan, Advanced oxidation of natural organic matter using hydrogen peroxide and iron-coated pumice particles, Chemosphere 68 (2007) 1846–1853.
[19] T. Liu, Z.L. Wang, X. Yan, B. Zhang, Removal of mercury (II) and chromium (VI) from wastewater using a new and effective composite: pumice-supported nanoscale zero-valent iron, Chem. Eng. J. 245 (2014) 34–40.
[20] T. Liu, L. Zhao, Z.L. Wang, Removal of hexavalent chromium from wastewater by $Fe^0$-nanoparticles-chitosan composite beads: characterization, kinetics and thermodynamics, Water Sci. Technol. 66 (5) (2012) 1044–1051.
[21] M.J. Alowitz, M.M. Scherer, Kinetics of nitrate, nitrite, and Cr (VI) reduction by iron metal, Environ. Sci. Technol. 36 (2002) 299–306.
[22] A.R. Iftikhar, H.N. Bhatti, M.A. Hanif, R. Nadeem, Kinetic and thermodynamic aspects of Cu (II) and Cr (III) removal from aqueous solutions using rose waste biomass, J. Hazard. Mater. 161 (2009) 941–947.
[23] L. Cumbal, J. Greenleaf, D. Leun, A.K. Sen-Gupta, Polymer supported inorganic nanoparticles: characterization and environmental applications, React. Funct. Polym. 54 (2003) 167–180.
[24] X.Q. Li, J.S. Cao, W.X. Zhang, Stoichiometry of Cr (VI) immobilization using nanoscale zerovalent iron (nZVI): a study with high-resolution X-ray photoelectron spectroscopy (HR-XPS), Ind. Eng. Chem. Res. 47 (2008) 2131–2139.
[25] J. Shen, Z. Li, Q. Yan, Y. Chen, Reaction of bivalent metal ions with borohydride in aqueous solution for preparation of ultrafine amorphous alloy particles, J. Phys. Chem. 97 (1993) 8504–8511.
[26] F. He, D.Y. Zhao, Manipulating the size and dispersibility of zerovalent iron nanoparticles by use of carboxymethyl cellulose stabilizers, Environ. Sci. Technol. 41 (17) (2007) 6216–6221.
[27] R.G. Shimmin, A.B. Schoch, P.V. Braun, Polymer size and concentration effects on the size of gold nanoparticles capped by polymeric thiol, Langmuir 20 (2004) 5613–5620.
[28] T. Liu, L. Zhao, X. Tan, S. Liu, J. Li, Y. Qi, G. Mao, Effects of physicochemical factors on Cr (VI) removal from leachate by zero-valent iron and $\alpha$-$Fe_2O_3$ nanoparticles, Water Sci. Technol. 61 (2010) 2759–2767.
[29] J.S. Cao, W.X. Zhang, Stabilization of chromium ore processing residue (COPR) with nanoscale iron particles, J. Hazard. Mater. 132 (2006) 213–219.
[30] N. Melitas, O. Chuffe-Moscoso, J. Farrell, Kinetics of soluble chromium removal from contaminated water by zerovalent iron media: corrosion inhibition and passive oxide effects, Environ. Sci. Technol. 35 (2001) 3948–3953.
[31] B.A. Manning, K. Jr, S.R. Kanel Hancheol-Kwon, Spectroscopic investigation of Cr (III) and Cr (VI)-treated nanoscale zero-valent iron, Environ. Sci. Technol. 41 (2007) 586–592.
[32] A. Benhammou, A. Yaacoubi, L. Nibou, B. Tanouti, Study of the removal of mercury (II) and chromium (VI) from aqueous solutions by Moroccan stevensite, J. Hazard. Mater. 117 (2005) 243–249.
[33] T.Y. Guo, Y.Q. Xia, G.J. Hao, M.D. Song, B.H. Zhang, Adsorptive separation of hemoglobin by molecularly imprinted chitosan beads, Biomaterials 25 (2004) 5905–5912.
[34] Z. Wu, C. Li, Kinetics and thermodynamics of $\beta$-carotene and chlorophyll adsorption onto acid-activated bentonite from Xinjinag in xylene solution, J. Hazard. Mater. 171 (2009) 582–587.
[35] V.K. Gupta, Equilibrium uptake, sorption dynamics, process development and column operations for the removal of copper and nickel from aqueous solution and wastewater using activated slag, a low-cost adsorbent, Ind. Eng. Chem. Res. 37 (1998) 192–202.
[36] Y.S. Ho, T.H. Chiang, Y.M. Hsueh, Removal of basic dye from aqueous solution using tree fern as a biosorbent, Process Biochem. 40 (2005) 119–124.
[37] S.Y.T. Muhammad-Choong, T.G. Chuah, R. Yunus, Y.H. Taufiq-Yap, Adsorption of $\beta$-carotene onto mesoporous carbon coated monolith in isopropyl alcohol and $n$-hexane solution: equilibrium and thermodynamic study, Chem. Eng. J. 164 (2010) 178–182.